# Three Distinct Modes of Exocytosis Revealed by Amperometry in Neuroendocrine Cells

G. Th. H. van Kempen,[†] H. T. vanderLeest,[†] R. J. van den Berg,[†] P. Eilers,[‡] and R. H. S. Westerink[§*]
[†]Department of Molecular Cell Biology, Leiden University Medical Center, Leiden, The Netherlands; [‡]Department of Biostatistics, Erasmus University, Rotterdam, The Netherlands; and [§]Neurotoxicology Research Group, Toxicology Division, Institute for Risk Assessment Sciences, Utrecht University, Utrecht, The Netherlands

ABSTRACT Neurotransmission requires $Ca^{2+}$-dependent release of secretory products through fusion pores that open and reclose (partial membrane distention) or open irreversibly (complete membrane distention). It has been challenging to distinguish between these release modes; however, in the work presented here, we were able to deduce different modes of depolarization-evoked exocytosis in neuroendocrine chromaffin and PC12 cells solely by analyzing amperometric recordings. After we determined the quantal size (Q), event half-width ($t_{50}$), event amplitude ($I_{peak}$), and event decay time constant ($\tau_{decay}$), we fitted scatter plots of log-transformed data with a mixture of one- and two-dimensional Gaussian distributions. Our analysis revealed three distinct and differently shaped clusters of secretory events, likely corresponding to different modes of exocytosis. Complete membrane distention, through fusion pores of widely varying conductances, accounted for 70% of the total amount of released catecholamine. Two different kinds of partial membrane distention (kiss-and-run and kiss-and-stay exocytosis), characterized by mode-specific fusion pores with unitary conductances, accounted for 20% and 10%, respectively. These results show that our novel one- and two-dimensional analysis of amperometric data reveals new release properties and enables one to distinguish at least three different modes of exocytosis solely by analyzing amperometric recordings.

## INTRODUCTION

Exocytosis, the merging of the cell membrane with the membrane of a neurotransmitter-filled vesicle, is essential for neurotransmission. Upon fusion, vesicles release their content in the extracellular space. Exocytosis is $Ca^{2+}$-dependent and is thought to occur by at least two mechanisms (1–3). First, all vesicle content is released through an irreversibly opened fusion pore, followed by collapse of the vesicle and integration of its membrane into the plasma membrane (complete membrane distention, often referred to as full fusion). Second, release occurs through formation of a reversible fusion pore that opens and closes again (partial membrane distention often referred to as kiss-and-run exocytosis). Partial membrane distention may be an adaptive mechanism to keep up with high-frequency stimulation. Additionally, it may aid in regulating the amount of neurotransmitter that is released per vesicle (quantal size (Q)), such that the open time and/or the diameter of the fusion pore will determine Q (3). Moreover, partial membrane distention could enable the differential release of proteins and classical neurotransmitters (4,5). Consequently, the regulation of different modes of exocytosis may be critical for neurotransmission and presynaptic plasticity (3).

For almost 20 years, investigators have used carbon-fiber microelectrode amperometry to measure exocytosis from single neuroendocrine cells (6). Amperometry has unparalleled sensitivity and time resolution, and has been successfully used to detect differences in the amount of neurotransmitter secreted per vesicle or in fusion kinetics, which are reflected in spike characteristics. Although morphological data are inconclusive, distinct populations of secretory events have been demonstrated by amperometry based on Q-values in both PC12 and chromaffin cells (7–9). These data indicate the existence of at least two types of secretory vesicles or two different modes of secretion. Previous analyses of amperometric spikes indicated that different modes of exocytosis could be reflected in several spike characteristics, such as the spike half-width or spike rise and decay time (10,11). Although this method offers the possibility of identifying different types of secretory events based on either the Q or the spike characteristics, the use of amperometry to distinguish different modes of exocytosis has been the subject of debate because it provides only indirect information about the state of the fusion pore and membrane fusion kinetics.

In recent years, researchers have developed sophisticated techniques, including patch-amperometry (12) and optical methods (13), to distinguish between complete and partial membrane distention. Results from these techniques have shown that both types of exocytosis occur in several types of secretory cells, although the relative preponderance of the different modes of exocytosis, as well as the apparent regulation by calcium levels, varies among cell types and species (12,14,15). However, a relatively simple and inexpensive way to distinguish these different modes of exocytosis would greatly facilitate studies of presynaptic plasticity and the function of specific proteins implicated in exocytosis.

Complete membrane distention is often considered an all-or-nothing event during which all content is released

*Submitted March 19, 2010, and accepted for publication January 4, 2011.*

*Correspondence: r.westerink@uu.nl

Editor: Lukas K. Tamm.



0006-3495/11/02/0968/10 $2.00

doi: 10.1016/j.bpj.2011.01.010

independently of the duration of the fusion event (but see Omiatek et al. 16)). In the case of partial membrane distention, however, vesicles release their content through a fusion pore of restricted diameter or open-time, or both. Cell-attached capacitance measurements indicated that the mean fusion pore open-time during partial membrane distention is usually in the range of tens or even hundreds of milliseconds (12,17,18). Unless the diameter of the fusion pore is severely restricted (4,5), it is presumed that the kinetics do not limit the amount of catecholamine (CA) that is released. However, very fast closure of the fusion pore (<2.5 ms) has been observed in chromaffin cells (12) and ventral midbrain neurons (19), suggesting that both the fusion pore open-time and fusion pore diameter can limit the amount of released CA. If the fusion pore open-time and/or diameter limit secretion, one would expect the amount of released neurotransmitter to be related to the open-time of the reversible fusion pore, and to observe a positive correlation between Q and the half-width ($t_{50}$) of the amperometric spike. Consequently, it must be possible to distinguish between complete and partial membrane distention based on several parameters of the amperometric events.

In this study, we investigated vesicular CA secretion in chromaffin and PC12 cells using amperometry, data transformation, and one- (1D) and two-dimensional (2D) Gaussian mixture analysis. Our data demonstrate the existence of at least three distinct clusters of exocytotic events that appear to be related to different modes of exocytosis: complete membrane distention and two modes of partial membrane distention (kiss-and-run and kiss-and-stay exocytosis). The results further indicate that each mode of exocytosis is characterized by mode-specific fusion pore properties that are similar for chromaffin and PC12 cells.

## MATERIALS AND METHODS

### Cell culture and chemicals

PC12 cells and mouse adrenal chromaffin cells were cultured as described previously (7,20). PC12 cells were used for experiments up to 20 passages. To augment the CA synthesis, PC12 cells were differentiated with 5 $\mu$M dexamethasone (Sigma-Aldrich, Zwijndrecht, The Netherlands) for 3–5 days (21).

### Carbon-fiber amperometry

We performed amperometric recordings to detect depolarization-evoked CA secretion, using 5 $\mu$m Ø ProCFE carbon-fiber electrodes (Dagan, Minneapolis, MN), essentially as described previously (7,20,21). Because it was previously shown that Q can increase as a result of exposure to high-$K^+$-containing saline (22), we made only one recording per culture dish. See the Supporting Material for further details.

### Event detection and selection

The amperometric recordings were digitally filtered at 1–2 kHz and then scanned for exocytotic events with the sliding-scale template in Clampfit 9 (Molecular Devices, Union City, CA). Two separate templates were used simultaneously to detect spikes and stand-alone-foot (SAF) events. Both templates have time courses characterized by rise time constants of ~0.5 ms to detect fast rising events with high sensitivity.

Cells were accepted for analysis if the number of events was >20. Several parameters were calculated from the detected events (Fig. 1 *B*),

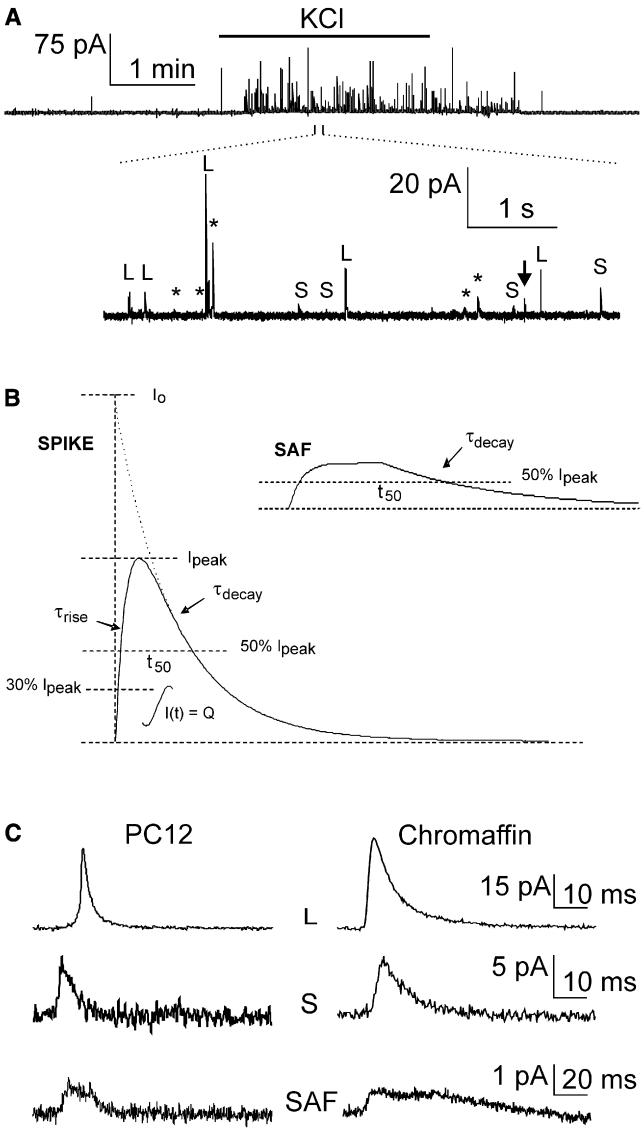


FIGURE 1 (*A*) Example amperometric recording, low-pass-filtered at 1 kHz, showing depolarization-evoked exocytosis of a PC12 cell during a 120 s application of 60 mM KCl-containing saline, indicated by the bar at the top of the recording. The lower part displays part of the amperometric recording on an expanded time and amplitude scale, illustrating the presence of S- and L-spikes as well as an SAF (*arrow*). Events indicated by an asterisk were discarded on the basis of the rise time. (*B*) Fusion events appear as spikes (*left*) and SAFs (*right*). Event characterization is based on the integrated charge (Q), peak amplitude ($I_{peak}$), the instantaneous current ($I_o$), rise time constant ($\tau_{rise}$) calculated from 30–60% of the peak, decay time constant ($\tau_{decay}$), and half-width ($t_{50}$). (*C*) Examples of large (L) and small (S) spikes and SAFs in PC12 (*left panel*) and chromaffin (*right panel*) cells on an expanded time and amplitude scale. The exocytotic events were classified according to the clustering procedures (see detailed explanation in the Supporting Material). The depicted events all originated very close to the detector, as evidenced by their small rise time constants.

including the integrated charge (Q, representing the number of CA molecules oxidized at the carbon surface), peak amplitude ($I_{peak}$), half-width ($t_{50}$), instantaneous current ($I_o$), rise time constant ($\tau_{rise}$, calculated from 30–60% from peak amplitude to avoid including the prespike foot), and decay time constant ($\tau_{decay}$). The $\tau_{rise}$ and $\tau_{decay}$ were both fitted with a single exponential function.

To avoid including fusion events that occurred too far away from the detecting electrode, and to guarantee complete detection of released CA, we excluded fusion events with $\tau_{rise} > 3$ ms (see Supporting Material for further details). In addition, we visually inspected all detected events to avoid acceptance of overlapping events. On average, 24% of the events were rejected, resulting in ~50 accepted exocytotic events per cell.

### Data analysis and statistics

For curve-fitting of the exocytotic currents, including prespike feet (PSFs; see Fig. S1 *B*, *inset*), we used exponential functions custom made in Clampfit 9 as detailed in the Supporting Material. We used log-transformed parameters throughout this study because many biological size distributions follow a log-normal distribution (23), and log-transformed values are an efficient means of comparing distributions of spike parameters (11,24–26). We fitted the 1D distributions of the log-transformed event parameters using functions of Origin7 software (OriginLab, Northampton, MA) to separate different types of exocytotic events. The 2D distributions of log-transformed relations between event parameters were used to separate different clusters of events. We fitted these Gaussian distributions using the expectation-maximization (EM) algorithm (27). For each component, three fitting options were allowed: a spherical shape (three parameters), an elliptic shape (four parameters), and an elliptic shape with arbitrary rotation (five parameters). A special-purpose program with a graphical user interface was written in MATLAB (The MathWorks, Natick, MA) to read the data, fit the model, and produce graphs and numerical reports. (This program is available on request.)

Whether the 1D or 2D distributions of (log-transformed) event parameters could be fitted with one, two, or three Gaussians functions was judged on the basis of Akaike's information criterion (AIC), which is given by $-2 \times \ln(L) + 2 \times K$, where L is the value of the log-likelihood and K is the number of free parameters. The best model is indicated by the lowest AIC value, and the difference between the AIC values obtained from the different models, rather than the absolute values, determines the best fit.

To more clearly visualize the resulting clusters of events, we assign different colors to the data points. Color images are made of the calculated distributions. The value of the fit for each individual data point (i.e., the probability that the data point belongs to a cluster) is multiplied by the respective cluster colors. Data points that are ambiguous in the fitted cluster separation will show an intermediate color.

Values represent the mean or median ± standard error (SE) from the number of cells ($n$) or events ($N$) indicated. Log-transformed data are compared via an independent $t$-test, with the level of significance ($p$) chosen as 0.05.

## RESULTS

### Spikes and SAFs

In most of the cells, depolarization evoked a burst of exocytosis (Fig. 1 *A*). The number of events was dependent on the extracellular $Ca^{2+}$ concentration, and events were not detected in $Ca^{2+}$-free solutions (not shown). Also, no events were detected after the carbon fiber was moved several micrometers away from the cell surface. After all events with $\tau_{rise} > 3$ ms (see Fig. S1 *B* and "Event detection and selection" section) were discarded, the amperometric data contained spikes as well as small foot-like events (i.e., SAFs; Fig. 1, *B* and *C*). In both PC12 and chromaffin cells, on average ~80% of the events were spikes and ~20% were SAFs.

To determine whether the events originated from distinct populations of vesicles and/or distinct modes of exocytosis, we collected a large number of amperometric events (spikes and SAFs) and calculated the distributions of several event parameters for both PC12 and chromaffin cells. Spikes (detected either by template matching or by threshold crossing) are relatively short-duration events with peak amplitudes exceeding ~2 pA. SAFs are small plateau-like events of only a few pA that presumably originate from the (fast) opening of a restricted (diameter) fusion pore without the final dilating step. After a variable time (usually tens of milliseconds), the steady current (slowly) declines to the baseline (cf. Fig. 1, *B* and *C*). Because SAFs have a low amplitude, they have been largely ignored in most studies. Note, however, that the onset of these fusion events is fast, with a median $\tau_{rise}$ of 0.9 ms and 1.4 ms for PC12 and chromaffin cells, respectively. Therefore, the $\tau_{rise}$-values of these small events are similar to those of the spikes, and thus arise close to the detecting carbon fiber.

### 1D Gaussian mixture analysis of spikes

Fig. 2 shows the distributions of the log-transformed values of Q (*A*), $I_{peak}$ (*B*), $\tau_{decay}$ (*C*), and $t_{50}$ (*D*) from pooled amperometric spikes of 17 PC12 cells (*left*) and 18 chromaffin cells (*right*). The distributions of Q are best fitted by the sum of two Gaussians. Moreover, except for the distribution of log $t_{50}$-values for PC12 cells (Fig. 2 *D*, *left*), all distributions, for both PC12 and chromaffin cells, are broad and best fitted with the sum of two Gaussians (as evidenced by the lower AIC and higher correlation coefficient than that obtained for a single Gaussian fit; see Table S2 for AIC values). The median values of the distinct populations are provided in Table 1.

Fig. 2 *A* indicates that there are two distinct populations of large ($Q_L$) and small ($Q_S$) quanta in both PC12 and chromaffin cells. This result is similar to our previous finding from an analysis of single-cell distributions (7), indicating that the two components in the distribution do not arise from pooling of the data. A similar distinction between large and small quanta is also evident from the bimodal distribution of log $I_{peak}$ (Fig. 2 *B*). Note that log Q (Fig. 2 *A*) is clearly shifted to larger values for chromaffin cells, although the range of spike amplitudes (Fig. 2 *B*) is rather comparable for PC12 and chromaffin cells. Distinct populations were also observed for the log-transformed distributions of $\tau_{decay}$ (Fig. 2 *C*). Although the distribution of $t_{50}$ is bimodal for chromaffin cells, this distribution is best described with a single Gaussian function in PC12 cells (Fig. 2 *D*), implying that the putative spike populations in PC12 cells have similar durations. Linear regression (not shown) indicated a strong positive correlation between Q and $I_{peak}$,

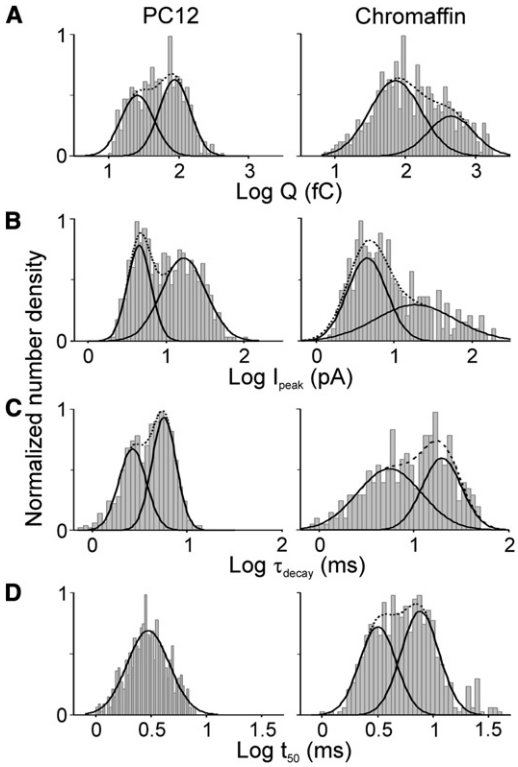


FIGURE 2 Distributions of spike parameters (depicted as *gray columns*) are number densities normalized on the maximum value. The solid lines represent the Gaussian functions fitted to the data, and the dashed line is the sum of the two functions. The best fit is obtained on the basis of the lowest AIC (see Table S2 for AIC values). Distributions of log Q (*A*), log $I_{peak}$ (*B*), log $\tau_{decay}$ (*C*), and log $t_{50}$ (*D*) are based on pooled data from 17 PC12 cells (544 events; *left*) and 18 chromaffin cells (560 events; *right*).

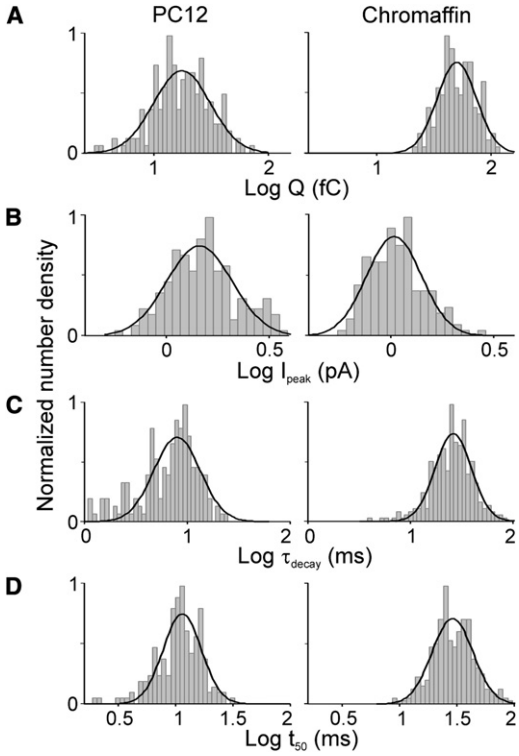


FIGURE 3 Distributions of SAF parameters of PC12 and chromaffin cells. Distributions (depicted as *gray columns*) are number densities normalized on the maximum value. The solid lines represent the single Gaussian functions fitted to the data (see Table S2 for AIC values). Distributions are based on pooled data from 17 PC12 cells (174 events; *left*) and 18 chromaffin cells (147 events; *right*).

and between Q and $t_{50}$, but a negative correlation between $I_{peak}$ and $\tau_{decay}$.

These combined results indicate that in PC12 and chromaffin cells, a population of large ($I_{peak}$ as well as Q) and rapidly decaying L-spikes coexists with a population of small ($I_{peak}$ as well as Q) and slower-decaying S-spikes, although both the L- and S-spikes originate close to the detector.

## 1D Gaussian mixture analysis of SAFs

Fig. 3 depicts the distributions of the log-transformed values of Q (*A*), $I_{peak}$ (*B*), $\tau_{decay}$ (*C*), and $t_{50}$ (*D*) from SAFs of PC12 and chromaffin cells. For both cell types, the distributions can be fitted reasonably with a single Gaussian (see Table 1 for median values and Table S2 for AIC values). Therefore, in contrast to the spikes, the data indicate that there is only a single population of SAFs. These SAFs have a smaller Q and event duration, and decay faster in PC12 cells compared with chromaffin cells, whereas $I_{peak}$ is comparable. It should be noted that SAFs, similar to spikes, originate close to the detector, as evidenced by their small $\tau_{rise}$.

**TABLE 1 Median values of the S-, L-, and SAF-event populations depicted in Figs. 2 and 3**

| | | Q (fC) | $I_{peak}$ (pA) | $\tau_{decay}$ (ms) | $t_{50}$ (ms) |
|---|---|---|---|---|---|
| PC12 | S | 25 | 4.5 | 5.7 | 3.0 |
| | L | 86 | 17 | 2.7 | 3.0 |
| | SAF | 18 | 1.5 | 8.0 | 12 |
| Chromaffin | S | 74 | 4.5 | 19.7 | 7.7 |
| | L | 465 | 20 | 5.5 | 3.2 |
| | SAF | 51 | 1.0 | 26.0 | 30 |

Of interest, the SAFs (see Table 1 for median values) are different from the PSFs, the plateau-like currents that frequently precede the spike phase of the secretory events and reflect the opening of a fusion pore just before further expansion. These PSFs are observed in ~70% of L-spikes but in only 10% of the S-spikes, in agreement with previous data (28) demonstrating that ~50% of the events with a large Q (i.e., L-events) have a PSF, whereas the occurrence of a PSF is near zero for events with a small Q (i.e., S-events). The median PSF duration in PC12 cells (6.2 ms) is significantly smaller than in chromaffin cells (8.7 ms; $p < 0.001$). However, their peak amplitudes are not significantly different, amounting to 5.7 pA in PC12 and 5.0 pA in chromaffin cells. Also, the median $\tau_{rise}$-values of the PSFs are not significantly different (3.9 and 2.9 ms for PC12 and chromaffin cells, respectively). Despite this relatively large

$\tau_{rise}$, the PSFs originate close to the detector, as the spikes that follow the PSF phase have small $\tau_{rise}$ of ~0.4 ms. This supports the view that in PC12 and chromaffin cells the PSF arises from the relatively slow formation of a not-yet-dilated fusion pore, which differs from the SAFs that appear to arise from fast formation of a nondilated fusion pore. The almost nonoverlapping distributions of the SAF and PSF amplitudes and kinetics suggest that these events derive from different underlying processes, and indicate the existence of different populations of fusion pores.

### 2D Gaussian mixture analysis of spikes and SAFs

To further investigate the presence of different event clusters and their properties, we analyzed the relations between event parameters by 2D Gaussian mixture analysis (see Supporting Material). For both spikes and SAFs, scatter plots of log Q versus log $I_{peak}$ (Fig. 4 *A*), log $I_{peak}$ versus log $\tau_{decay}$ (Fig. 4 *B*), and log Q versus log $t_{50}$ (Fig. 4 *C*) were fitted with mixtures of 2D Gaussian functions. These fittings revealed the presence of three distinct event clusters: L- and S-spikes and SAFs (Fig. 4; see Table S3 for AIC values). Similar results were obtained from the separate fittings of the event relations from the spikes, revealing the S- and L-clusters (Fig. S2), and from the SAFs, yielding a single cluster of SAF events (Fig. S3).

Clusters identified in PC12 cells are remarkable similar to chromaffin cells. Each fitted cluster is assigned a Gaussian with its median in the center of the cluster and with a standard deviation that measures the spread of the cluster. The median center values of the clusters are given in Table 2. Of importance, the centers obtained from the 2D mixture analyses correspond well (by a factor of $<2$) with the median values from the 1D distributions of these spike parameters (Figs. 2 and 3). The same three clusters were also obtained when only the first 10 or last 10 events per cell were analyzed (Fig. S4), which indicates that the distinct clustering was not due to changes in Q or $t_{50}$ over time. Although it is probably more likely that pooling of the data would obscure the different clusters, data from individual cells were also analyzed to exclude the possibility that the clustering was due to pooling data of several cells. Analysis of data from individual cells revealed similar clusters (Fig. S5), although the clusters were sometimes incomplete due to the relatively small number of events per cell.

Plotting log Q as a function of log $I_{peak}$ (Fig. 4 *A*) indicates that Q and $I_{peak}$ are directly proportional for S- and L-events as well as for SAFs. In both types of cells, SAFs contributed ~20% to the total number of events, whereas L- and S-events contributed ~45% and 35%, respectively. For both PC12 and chromaffin cells, the Q of S-spikes is significantly smaller than that of L-spikes, but larger than that of SAFs ($p < 0.0001$). Similarly, the $I_{peak}$ of S-spikes is significantly smaller than that of L-spikes, but larger than that of SAFs ($p < 0.0001$; see Table 2). The median

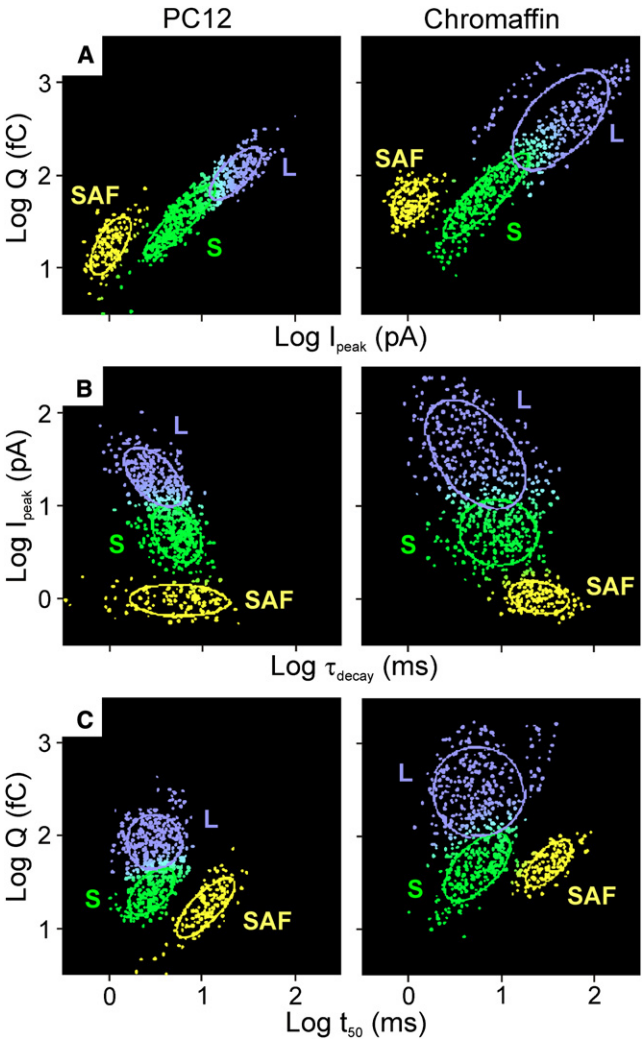


FIGURE 4 2D Gaussian mixture analysis of the relations between event parameters of PC12 and chromaffin cells (spikes and SAFs): log Q vs. log $I_{peak}$ (*A*), log $I_{peak}$ vs. log $\tau_{decay}$ (*B*), and log Q vs. log $t_{50}$ (*C*). The scatter plots contain the pooled data from 17 PC12 cells (689 events; *left*) and 18 chromaffin cells (707 events; *right*). Three 2D Gaussian distributions (denoted by L, S, and SAF) were fitted to the data, yielding the different cluster centers (center ordinate, center abscissa). Solid lines represent the variance of the clusters. Correlation coefficients were calculated from the fit. Linear regression of the fitted clusters yields the slope of the cluster. For all scatter plots, the best fit is obtained on the basis of the lowest AIC ($AIC_{3\ Gausians} < AIC_{2\ Gaussian}$); see Table S3 for AIC values. SAFs contribute ~20% of the total number of events. See Table 2 for center values, slopes, and correlation coefficients of the different clusters.

peak amplitudes of S-events and SAFs of PC12 and chromaffin cells are remarkably similar, although in the latter, the mean Q for S-events and SAFs is ~2–3 times larger. From the position of the clusters along the abscissa, it follows that the separation between the S- and L-clusters lies around 15 pA, i.e., events with peaks $>$ 15 pA are predominantly L-events in both types of cells.

When log $I_{peak}$ is plotted as a function of log $\tau_{decay}$ (Fig. 4 *B*), an approximately inversely proportional relation between $I_{peak}$ and $\tau_{decay}$ is found for L-events, indicating

**TABLE 2 Median values of S, L, and SAF clusters based on three 2D Gaussian functions depicted in Fig. 4 for (*A*) Log Q-log $I_{peak}$, (*B*) Log $I_{peak}$-log $\tau_{decay}$, and (*C*) Log Q-log $t_{50}$**

| | S | | L | | SAF | |
|---|---|---|---|---|---|---|
| (*A*) Log Q - log $I_{peak}$ | mcv | sl/r | mcv | sl/r | mcv | sl/r |
| PC12 | 32.6fC-5.9pA | 1/0.89 | 104.9fC-23.1pA | 1/0.71 | 17.6fC–1.0pA | 1.7/0.64 |
| Chromaffin | 60.0fC-7.0pA | 1/0.87 | 396.4fC-44.3pA | 1/0.58 | 51.3fC–1.1pA | 1.4/0.31 |
| (*B*) Log $I_{peak}$ - log $\tau_{decay}$ | | | | | | |
| PC12 | 5.0pA–5.2ms | −1.6/−0.34 | 20.3pA–3.0ms | −1.0/−0.53 | 1.0pA–5.5ms | −0.04/−0.11 |
| Chromaffin | 5.2pA–9.3ms | −0.14/−0.04 | 36.3pA–5.2ms | −1.3/−0.44 | 1.0pA–25.1ms | −0.19/−0.25 |
| (*C*) Log Q − log $t_{50}$ | | | | | | |
| PC12 | 25.0fC–2.9ms | 1/0.55 | 85.6fC–3.0ms | spherical/<0.2 | 16.7fC–10.9ms | 1/0.75 |
| Chromaffin | 46.6fC–5.5ms | 1/0.59 | 304.6fC–5.6ms | spherical/<0.2 | 51.2fC–32.3ms | 1/0.65 |

Values correspond to the median center values (mcv; left) and slopes (sl) and correlation coefficient (r; right) of the different event clusters in PC12 and chromaffin cells.

that a large L-spike will thus decay faster than a smaller L-spike. For S-events and SAFs, $I_{peak}$ and $\tau_{decay}$ are hardly correlated ($r \leq 0.3$). For both cell types, the $I_{peak}$ of S-spikes is significantly smaller than that of L-spikes, but larger than that of SAFs ($p < 0.0001$). The median $\tau_{decay}$ of S-spikes is significantly larger than that of L-spikes, but smaller than that of SAFs ($p < 0.0001$; see Table 2).

The relation between log Q and log $t_{50}$ is plotted in Fig. 4 *C*. For L-events, log Q and log $t_{50}$ are hardly correlated ($r < 0.2$), indicating that Q and the half-width are not (or are only weakly) related. The Q-values of the S-spikes and SAFs are approximately proportional to $t_{50}$. The median Q of S-spikes is significantly smaller than that of L-spikes ($p < 0.0001$). In PC12 cells, the Q of SAFs is even smaller than that of S-spikes ($p < 0.0001$), whereas in chromaffin cells the SAFs and S-spikes have a comparable Q. The median $t_{50}$ of S- and L-spikes are very similar, though much smaller than that of SAFs ($p < 0.0001$; see Table 2).

The center values of $I_{peak}$ of the different clusters found in the log Q-log $I_{peak}$ scatter plots (Fig. 4 *A*) correspond well with the centers obtained from the clusters found in the log $I_{peak}$-log $\tau_{decay}$ plot (Fig. 4 *B*). Similarly, the center values found in the log Q-log $I_{peak}$ scatter plots (Fig. 4 A) correspond well with the centers obtained from the clusters found in the log Q-log $t_{50}$ plot (Fig. 4 *C*). This indicates that from fitting the log Q-log $I_{peak}$, log $I_{peak}$-log $\tau_{decay}$ or log Q-log $t_{50}$ the same clusters of L-, S- and SAF-events are identified. This strongly supports the view that in both PC12 and chromaffin cells a distinct population of L-spikes (large Q and $I_{peak}$, small $\tau_{decay}$) coexists with distinct populations of S-spikes (small Q and $I_{peak}$, large $\tau_{decay}$) and SAFs (very small Q, small $I_{peak}$, very large $\tau_{decay}$ and $t_{50}$), which can be separated by a quantitative event analysis. These clusters differ not only in Q, $I_{peak}$, and decay kinetics but also in their relation between $I_{peak}$ and $\tau_{decay}$, and between Q and $t_{50}$. In our view, the different relations between the parameters of the different event clusters reflect different modes of exocytosis (see Discussion).

### In contrast to L-events, SAF- and S-events are characterized by unitary currents

A linear relation between Q and $t_{50}$ is expected for secretory vesicles that contain similar concentrations of free CA and empty through restricted (open-time or duration) fusion pores of unitary conductance (Eq. 1) (29,30). To estimate the conductance of the open fusion pore, we estimated the current $I_o$ that would flow if the dilated fusion pore were to open instantaneously (cf. Fig. 1 *B*). This new parameter is uncontaminated by changes in the free intra- and extravesicular CA concentrations, because directly after the actual opening of the fusion pore, [CA] drops from its initial value ($[CA]_o$). The magnitude of $I_o$ is determined only by the conductance of the dilated fusion pore and $[CA]_o$ at the moment of fusion pore opening (29). For SAFs, the parameter $I_o$ is identical to their $I_{peak}$. Fig. 5 shows the obtained $I_o$ distributions for the L-, S-, and SAF-events, and reveals remarkably similar results for PC12 cells (Fig. 5 *A*) and chromaffin cells (Fig. 5 *B*). The $I_o$ distribution of L-events is extremely broad, ranging from 10 to >100 pA, whereas the S- and SAF-events exhibit almost nonoverlapping distributions centered around 10 and 2 pA, respectively. The wide distribution of the $I_o$-values of the L-events indicates that either the dilated fusion pores have widely varying conductances or $[CA]_o$ varies strongly between vesicles, or both. However, experimental data suggest that $[CA]_o$ is tightly regulated (31–33), and therefore it is more probable that the conductance of these fusion pores varies largely. Likewise, the (restricted) fusion pores underlying the S- and SAF-events have unitary conductances.

## DISCUSSION

Previous studies have revealed different modes of exocytosis with the use of sophisticated techniques (12–14). However, the results presented here demonstrate that one can distinguish different modes of exocytosis solely by analyzing amperometric recordings. From these

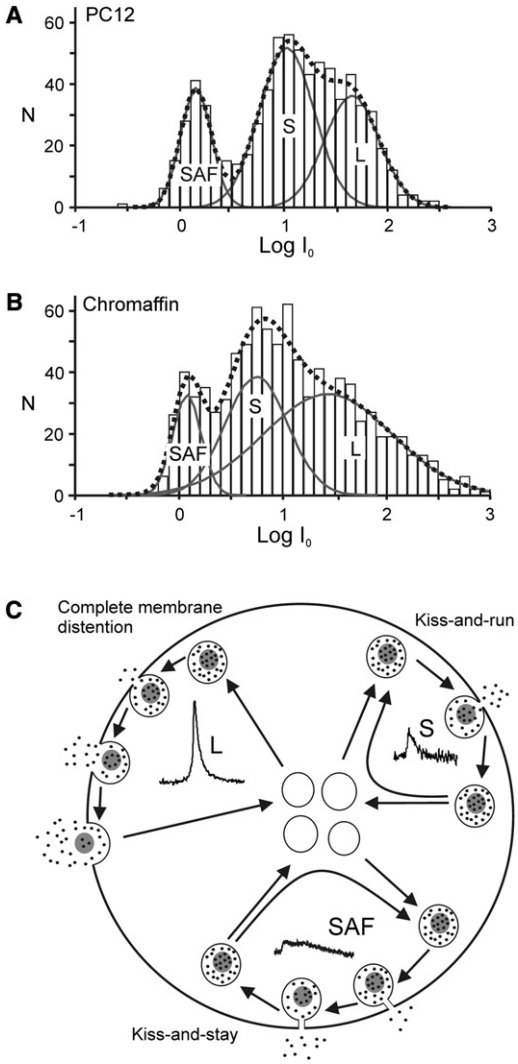


FIGURE 5 Normalized distribution of log-transformed instantaneous currents $I_o$ underlying SAF-, S-, and L-events in PC12 (*A*) and chromaffin (*B*) cells. The instantaneous currents $I_o$ were obtained from events of Fig. 4 *A*, classified in the indicated clusters. The magnitude of $I_o$ is given by a modification of Eq. 4 in Almers et al. (29): $I_o = n_e F \rho D [CA]_o \gamma$, where $n_e$ is the number of electrons in the electrochemical oxidation of one CA molecule, F is Faraday's constant, $\rho$ is the resistivity of the pore lumen, D is the diffusion coefficient, and $[CA]_o$ is the intravesicular free CA concentration before the fusion pore, with conductance $\gamma$, opens. (*C*) Diagrammatic summary of different modes of exocytosis by SAF-, S-, and L-vesicles. SAF-vesicles show kiss-and-stay exocytosis by restricted fusion pores of very small unitary currents ($I_o \sim 2$ pA). S-vesicles perform kiss-and-run exocytosis through dilated fusion pores of unitary currents ($I_o \sim 10$ pA) that reclose very rapidly, whereas L-vesicles exhibit complete secretion through dilated fusion pores with largely varying currents ($I_o \sim 10 - >100$ pA).

amperometric recordings, we were able to visualize three distinct populations of secretory events in intact neuroendocrine chromaffin and PC12 cells using 1D and 2D distributions of event characteristics. These distinct 1D and 2D distributions and their different shapes of event clusters indicate that the distinct populations likely correspond to separate modes of exocytosis, possibly representing distinct populations of secretory vesicles. It is clear that in chromaffin cells, as compared with PC12 cells, the event clusters are shifted to larger half-widths and to larger released quantities, evidently related to slower kinetics and larger vesicles. The shapes of the distinct populations of secretory events, however, are remarkably comparable between PC12 and chromaffin cells (Figs. 2–5).

The 1D distributions of event parameters (Q, $I_{peak}$, $\tau_{decay}$, and $t_{50}$) clearly indicate the presence of at least two populations of secretory spikes (Fig. 2) as well as a single population of low-amplitude SAFs (Fig. 3). These three populations of secretory events are also clearly distinguishable in the 2D Gaussian mixture analysis (Fig. 4), further supporting the existence of distinct populations of secretory events in both PC12 and chromaffin cells. Of note, the center values obtained from the 2D mixture analysis are also comparable (deviating by a factor of $<2$) to the median values obtained from the 1D distributions, and thus represent the same populations (Tables 1 and 2). It is essential to point out that the 2D analyses of events from single cells revealed similar but sometimes incomplete clusters of events (Fig. S6), demonstrating that clustering did not originate from pooling events from different cells.

It is important to note that the measured amperometric L-, S-, and SAF-events originate close to the detector. This is strongly supported by their small rise time constants. Selecting for fast rise times ($\tau_{rise} < 3$ ms) is regarded as an accurate way to estimate charge, because mainly events from near sites are included (34). Consequently, it is unlikely that event kinetics will be contaminated by events that partially escape complete oxidation of the released CA due to fusion at a site relatively far from the electrode (34). Using a $\tau_{rise} > 3$ ms as the only exclusion criterion likely adds to the observed contrast of the different distributions. Of note, selection on the basis of the event amplitude (e.g., an amplitude threshold of 5 pA, as is often used) is not satisfactory because it excludes all low-amplitude SAFs as well as a considerable fraction of S-events. Another factor that likely contributes to the clearly distinguishable distributions is the use of log-transformed values, which was previously shown to be an efficient way to compare distributions of spike parameters (11,24). Moreover, in our analysis, SAFs were separated from the spike-like S- and L-events, whereas SAFs may have been included occasionally in previous distributions because SAFs and S-events have rather comparable Q- and $I_{peak}$-values. Inclusion of SAFs could cause a broader distribution in the low-Q range and make it more difficult to distinguish the different distributions. In addition, using only events recorded during the first depolarization may increase contrast. The largest contrast is achieved by using 2D distributions of log-transformed spike parameters instead of 1D distributions of nontransformed values.

The observed event populations differ in several aspects, and it is likely that these different populations differ in fusion (pore) properties and may even represent distinct populations of vesicles. Although the $t_{50}$-values of L- and S-events are rather comparable, L-events have a large Q and $I_{peak}$ and a small $\tau_{decay}$, whereas S-events have a small Q and $I_{peak}$ and a large $\tau_{decay}$. SAFs have a small Q and a very small $I_{peak}$, although $t_{50}$ and $\tau_{decay}$ are very large. For L-, S-, and SAF-events, the amount of CA released (Q) is proportional to their peak value ($I_{peak}$). Of importance, the event populations differ prominently in their $I_{peak}$-$\tau_{decay}$ and Q-$t_{50}$ relations. $I_{peak}$ is inversely proportional to $\tau_{decay}$ for L-events, but is essentially unrelated to $\tau_{decay}$ for S- and SAF-events. Q and $t_{50}$ are unrelated in L-events but are proportional for both S-events and SAFs (Fig. 4).

The three event clusters release CAs at very different rates ($I_{peak}$), which are either inversely related to or unrelated to $\tau_{decay}$ (Fig. 4 *B*). The presence or absence of an inverse relation between $I_{peak}$ and $\tau_{decay}$ (Fig. 4 *B*) can simply be related to different properties of the fusion pore. For a vesicle with volume *V*, where all CA is in free solution and the fusion pore opens instantly with a conductance $\gamma$, the decay time constant of release is given by:

$$\tau_{decay} = \frac{V}{\rho D \gamma} \quad (1)$$

where $\rho$ represents the resistivity of the fusion pore lumen and *D* represents the diffusion coefficient (29). Thus, $\tau_{decay}$ is independent of [CA] and is determined only by the vesicle volume *V* and pore conductance $\gamma$, irrespective of whether the vesicle is completely or partially filled. Equation 1 predicts an inverse relation between $\tau_{decay}$ and fusion pore conductance $\gamma$. If pores that form during fusion exhibit widely varying conductances, an inverse relation between $I_{peak}$ and $\tau_{decay}$ can thus be expected for L-events. On the other hand, if the pore conductance is not variable but exhibits more or less unitary properties, such a relation will be absent for S- and SAF-events (Fig. 4 *B*).

In a recent study, Omiatek et al. (16) reported that vesicles release on average only ~40% of their total neurotransmitter content, and that complete membrane distention is uncommon. However, it seems reasonable to assume that during complete membrane distention (L-events), all intravesicular CAs will be released independently of the duration of this catastrophic event. The apparent absence of complete secretion of all intravesicular CAs noted by Omiatek et al. (16) may indicate that their recording or culture conditions favored partial membrane distention. The large variations in the fusion pore conductance underlying L-events (Fig. 5) may originate from dilation of narrow and wide fusion pores during the catastrophic process of complete membrane distention. These L-events, which under our conditions represent ~40% of the fusion events, are characterized by a very poor correlation between log Q and log $t_{50}$ (Fig. 4 *C*), suggesting a complete release of vesicular content during complete membrane distention.

In our view, however, S- and SAF-events show putative characteristics of partial membrane distention with a restricting fusion pore. When the fusion pore acts as a limiting factor (restricted open-time and/or diameter), we would expect the amount of released CA to be related to the open-time of the unitary conducting fusion pore. Consequently, the longer the fusion pore stays open, the more CA will be released, and Q would be expected to be proportional to $t_{50}$ if the fusion pore closes before the vesicle is completely emptied (35). Moreover, complete release through fusion pores with unitary conductances would also result in such dependence (30). The observed relations between Q and $t_{50}$ for both the S- and SAF-vesicle populations (Fig. 4), as well as their unitary conductances (Fig. 5), are consistent with these predictions.

Although we observed similarities between S- and SAF-events, we also observed several differences. The main differences were the long duration and very slow decay of the SAFs, and the very low value of $I_o$ for SAFs. The narrow distribution of $I_o$-values for S-events and SAFs (Fig. 5) indicates the existence of pores with unitary conductances, probably representing molecular structures with fixed pore diameters. The instantaneous currents $I_o$ of S-events are clearly larger than those of SAFs and even overlap with those of L-events. Given that log Q and log $t_{50}$ are unrelated in L-events, it is unlikely that the diameter of these fusion pores is limiting the amount of CA secreted. Yet, for S-events, a positive correlation between log Q and log $t_{50}$ is evident. If the fusion pore diameter is not restricting, then the most likely limiting factor is the open-time of the fusion pore. This is in line with reports of very fast closure (<2.5 ms) of the fusion pore in chromaffin cells (12,36) and ventral midbrain neurons (19).

On the other hand, considering the slow time course of their decay, it is rather unlikely that SAFs are compatible with a fast mode of partial membrane distention. It is more likely that SAFs secrete their content through a very low conducting pore (5) of constant magnitude that stays open for a long duration (12,17,18), slowly clearing the vesicle (kiss-and-stay). Because the speed of release is very limited for these SAF-events, the large, dense core of the vesicle most likely acts as a CA reservoir that keeps the free intravesicular [CA] constant during the steady-state phase of the events. Amperometric recordings from dialyzed, whole-cell, patch-clamped chromaffin cells revealed SAFs with a similar slow decay (36).

The picture that thus emerges is one of vesicles undergoing complete membrane distention and exhibiting fusion pores with widely varying conductances (L), in contrast to vesicles undergoing partial membrane distention and forming fusion pores with relatively unitary conductances (S and SAF; Fig. 5, *inset*). The positive correlation between log Q and log $t_{50}$ indicates that fusion pore characteristics restrict

CA secretion for S-events and SAFs. The very limited open-time of the fusion pore restricts S-events (kiss-and-run), whereas SAFs are restricted by the very low conductance of the fusion pore (kiss-and-stay).

Although S-events occur as frequently as L-events during depolarization-evoked exocytosis, the latter contribute for the most part to the amount of CA released in both types of neuroendocrine cells. In both chromaffin and PC12 cells, complete membrane distention, kiss-and-run, and kiss-and-stay contribute on average ~70%, ~20%, and ~10%, respectively, to the total amount of released CA.

It is widely accepted that there are two modes of exocytosis, which are usually referred to as full fusion (complete membrane distention) and kiss-and-run exocytosis (partial membrane distention). The occurrence of SAFs is usually attributed to kiss-and-run exocytosis. However, our data suggest that the form of partial membrane distention associated with SAFs is a rather slow mode of exocytosis that may more accurately be referred to as kiss-and-stay, whereas the spike-like S-events, which most likely reflect a very rapid mode of partial membrane distention, could be referred to as true kiss-and-run events.

The occurrence of different modes of exocytosis appears to be at least partly regulated by the level of intracellular $Ca^{2+}$ a vesicle experiences (12,14), by protein phosphorylation (10), and by the molecular composition of the release sites and/or vesicle-specific properties (9). Previous imaging experiments suggested the existence of different modes of exocytosis characterized by different-sized fusion pores, with the smallest having a very restricted pore diameter (37). Moreover, Vardjan et al. (5) proposed three different types of fusion pores with diameters of 0.5 nm, 1 nm, and $>3$ nm, respectively. Of note, Albillos et al. (32) suggested that a vesicle with a fusion pore $< 3$ nm likely retains its dense core.

Because $I_{peak}$ reflects the CA concentration at postsynaptic target receptors, it is tempting to speculate that the almost rectangular-shaped, low-amplitude, long-duration SAF-events, which likely retain their dense core, have a neuromodulatory role, whereas the spike-like S- and L-events allow for quantal neurotransmission. Switching between the different modes of exocytosis would provide an appealing mechanism for modulating Q and presynaptic plasticity. The ability to easily distinguish between the different modes of exocytosis by analyzing amperometric recordings would strongly facilitate the search for the precise underlying mechanisms.

## SUPPORTING MATERIAL

Supporting text, five figures, and three tables are available at http://www.biophysj.org/biophysj/supplemental/S0006-3495(11)00055-5.

We thank Drs. S. Michel and J. J. Plomp for helpful discussions, Ing. A. de Groot for technical assistance, and Prof. T. Stijnen for statistical advice.

## REFERENCES

1. Fernández-Peruchena, C., S. Navas, …, G. Alvarez de Toledo. 2005. Fusion pore regulation of transmitter release. *Brain Res. Brain Res. Rev.* 49:406–415.
2. Harata, N. C., A. M. Aravanis, and R. W. Tsien. 2006. Kiss-and-run and full-collapse fusion as modes of exo-endocytosis in neurosecretion. *J. Neurochem.* 97:1546–1570.
3. Westerink, R. H. 2006. Targeting exocytosis: ins and outs of the modulation of quantal dopamine release. *CNS Neurol. Disord. Drug Targets.* 5:57–77.
4. Perrais, D., I. C. Kleppe, …, W. Almers. 2004. Recapture after exocytosis causes differential retention of protein in granules of bovine chromaffin cells. *J. Physiol.* 560:413–428.
5. Vardjan, N., M. Stenovec, …, R. Zorec. 2007. Subnanometer fusion pores in spontaneous exocytosis of peptidergic vesicles. *J. Neurosci.* 27:4737–4746.
6. Leszczyszyn, D. J., J. A. Jankowski, …, R. M. Wightman. 1990. Nicotinic receptor-mediated catecholamine secretion from individual chromaffin cells. Chemical evidence for exocytosis. *J. Biol. Chem.* 265:14736–14737.
7. Westerink, R. H., A. de Groot, and H. P. Vijverberg. 2000. Heterogeneity of catecholamine-containing vesicles in PC12 cells. *Biochem. Biophys. Res. Commun.* 270:625–630.
8. Grabner, C. P., S. D. Price, …, A. P. Fox. 2005. Mouse chromaffin cells have two populations of dense core vesicles. *J. Neurophysiol.* 94:2093–2104.
9. Tang, K. S., N. Wang, …, F. W. Tse. 2007. Influence of quantal size and cAMP on the kinetics of quantal catecholamine release from rat chromaffin cells. *Biophys. J.* 92:2735–2746.
10. Graham, M. E., D. W. O'Callaghan, …, R. D. Burgoyne. 2002. Dynamin-dependent and dynamin-independent processes contribute to the regulation of single vesicle release kinetics and quantal size. *Proc. Natl. Acad. Sci. USA.* 99:7124–7129.
11. Bretou, M., C. Anne, and F. Darchen. 2008. A fast mode of membrane fusion dependent on tight SNARE zippering. *J. Neurosci.* 28:8470–8476.
12. Alés, E., L. Tabares, …, G. Alvarez de Toledo. 1999. High calcium concentrations shift the mode of exocytosis to the kiss-and-run mechanism. *Nat. Cell Biol.* 1:40–44.
13. An, S., and D. Zenisek. 2004. Regulation of exocytosis in neurons and neuroendocrine cells. *Curr. Opin. Neurobiol.* 14:522–530.
14. Elhamdani, A., F. Azizi, and C. R. Artalejo. 2006. Double patch clamp reveals that transient fusion (kiss-and-run) is a major mechanism of secretion in calf adrenal chromaffin cells: high calcium shifts the mechanism from kiss-and-run to complete fusion. *J. Neurosci.* 26:3030–3036.
15. Taraska, J. W., and W. Almers. 2004. Bilayers merge even when exocytosis is transient. *Proc. Natl. Acad. Sci. USA.* 101:8780–8785.
16. Omiatek, D. M., Y. Dong, …, A. G. Ewing. 2010. Only a fraction of quantal content is released during exocytosis as revealed by electrochemical cytometry of secretory vesicles. *ACS Chem. Neurosci.* 1:234–245.
17. Neco, P., C. Fernández-Peruchena, …, E. Alés. 2008. Myosin II contributes to fusion pore expansion during exocytosis. *J. Biol. Chem.* 283:10949–10957.
18. Zhang, Z., Z. Zhang, and M. B. Jackson. 2010. Synaptotagmin IV modulation of vesicle size and fusion pores in PC12 cells. *Biophys. J.* 98:968–978.
19. Staal, R. G., E. V. Mosharov, and D. Sulzer. 2004. Dopamine neurons release transmitter via a flickering fusion pore. *Nat. Neurosci.* 7:341–346.
20. Westerink, R. H., M. B. Rook, …, W. J. Wadman. 2006. Dual role of calbindin-$_{D28K}$ in vesicular catecholamine release from mouse chromaffin cells. *J. Neurochem.* 99:628–640.

21. Westerink, R. H., and H. P. Vijverberg. 2002. Ca(2+)-independent vesicular catecholamine release in PC12 cells by nanomolar concentrations of Pb(2+). *J. Neurochem.* 80:861–873.

22. Pothos, E. N., E. Mosharov, …, D. Sulzer. 2002. Stimulation-dependent regulation of the pH, volume and quantal size of bovine and rodent secretory vesicles. *J. Physiol.* 542:453–476.

23. Sokal, R. R., and J. F. Rohlf. 1981. Biometry: the Principles and Practice of Statistics in Biological Research. W. H. Freeman and Company, San Francisco.

24. Sørensen, J. B., R. Fernández-Chacón, …, E. Neher. 2003. Examining synaptotagmin 1 function in dense core vesicle exocytosis under direct control of $Ca^{2+}$. *J. Gen. Physiol.* 122:265–276.

25. Van der Kloot, W. 1991. The regulation of quantal size. *Prog. Neurobiol.* 36:93–130.

26. Pothos, E. N., S. Przedborski, …, D. Sulzer. 1998. D2-like dopamine autoreceptor activation reduces quantal size in PC12 cells. *J. Neurosci.* 18:5575–5585.

27. McLachlan, G. J., and D. Peel. 2000. Finite Mixture Models. John Wiley & Sons, New York.

28. Amatore, C., S. Arbault, …, L. A. Sombers. 2005. Correlation between vesicle quantal size and fusion pore release in chromaffin cell exocytosis. *Biophys. J.* 88:4411–4420.

29. Almers, W., L. J. Breckenridge, and A. E. Spruce. 1989. The mechanism of exocytosis during secretion in mast cells. *In* Secretion and its Control. G. Oxford, and G. M. Armstrong, editors. Rockefeller University Press, Woods Hole. 269–282.

30. Wightman, R. M., T. J. Schroeder, …, K. Pihel. 1995. Time course of release of catecholamines from individual vesicles during exocytosis at adrenal medullary cells. *Biophys. J.* 68:383–390.

31. Colliver, T. L., S. J. Pyott, …, A. G. Ewing. 2000. VMAT-mediated changes in quantal size and vesicular volume. *J. Neurosci.* 20:5276–5282.

32. Albillos, A., G. Dernick, …, M. Lindau. 1997. The exocytotic event in chromaffin cells revealed by patch amperometry. *Nature.* 389:509–512.

33. Gong, L. W., I. Hafez, …, M. Lindau. 2003. Secretory vesicles membrane area is regulated in tandem with quantal size in chromaffin cells. *J. Neurosci.* 23:7917–7921.

34. Haller, M., C. Heinemann, …, E. Neher. 1998. Comparison of secretory responses as measured by membrane capacitance and by amperometry. *Biophys. J.* 74:2100–2113.

35. Burgoyne, R. D., and J. W. Barclay. 2002. Splitting the quantum: regulation of quantal release during vesicle fusion. *Trends Neurosci.* 25:176–178.

36. Zhou, Z., S. Misler, and R. H. Chow. 1996. Rapid fluctuations in transmitter release from single vesicles in bovine adrenal chromaffin cells. *Biophys. J.* 70:1543–1552.

37. Tsuboi, T., and G. A. Rutter. 2003. Multiple forms of "kiss-and-run" exocytosis revealed by evanescent wave microscopy. *Curr. Biol.* 13:563–567.